The FEBS Journal

FEBS PRESS science publishing by scientists

Metabolic heterogeneity of human hepatocellular carcinoma: implications for personalized pharmacological treatment

Nikolaus Berndt[1], Johannes Eckstein[2], Niklas Heucke[3], Tilo Wuensch[3], Robert Gajowski[4,5], Martin Stockmann[3], David Meierhofer[4] and Hermann-Georg Holzhütter[2]

1 Institute for Imaging Science and Computational Modelling in Cardiovascular Medicine, Charité – Universitätsmedizin Berlin, corporate member of Freie Universität Berlin, Humboldt-Universität zu Berlin, and Berlin Institute of Health, Germany
2 Institute of Biochemistry, Charité – Universitätsmedizin Berlin, corporate member of Freie Universität Berlin, Humboldt-Universität zu Berlin, and Berlin Institute of Health, Germany
3 Department of Surgery, Charité – Universitätsmedizin Berlin, corporate member of Freie Universität Berlin, Humboldt-Universität zu Berlin, and Berlin Institute of Health, Germany
4 Mass Spectroscopy Facility, Max Planck Institute for Molecular Genetics, Berlin, Germany
5 Department of Biology, Chemistry, and Pharmacy, Freie Universität Berlin, GermanyOpen access funding enabled and organized by ProjektDEAL.

Keywords
kinetic modeling; liver; mathematical model; metabolism; tumor metabolism

Correspondence
N. Berndt, Charité – Universitätsmedizin Berlin, Charitéplatz 1, 10117 Berlin, Germany
Tel: +49 30 450 528466
E-mail: nikolaus.berndt@charite.de

(Received 17 April 2020, revised 1 September 2020, accepted 5 October 2020)

doi:10.1111/febs.15587

Metabolic reprogramming is a characteristic feature of cancer cells, but there is no unique metabolic program for all tumors. Genetic and gene expression studies have revealed heterogeneous inter- and intratumor patterns of metabolic enzymes and membrane transporters. The functional implications of this heterogeneity remain often elusive. Here, we applied a systems biology approach to gain a comprehensive and quantitative picture of metabolic changes in individual hepatocellular carcinoma (HCC). We used protein intensity profiles determined by mass spectrometry in samples of 10 human HCCs and the adjacent noncancerous tissue to calibrate Hepatokin1, a complex mathematical model of liver metabolism. We computed the 24-h profile of 18 metabolic functions related to carbohydrate, lipid, and nitrogen metabolism. There was a general tendency among the tumors toward downregulated glucose uptake and glucose release albeit with large intertumor variability. This finding calls into question that the Warburg effect dictates the metabolic phenotype of HCC. All tumors comprised elevated β-oxidation rates. Urea synthesis was found to be consistently downregulated but without compromising the tumor's capacity for ammonia detoxification owing to increased glutamine synthesis. The largest intertumor heterogeneity was found for the uptake and release of lactate and the size of the cellular glycogen content. In line with the observed metabolic heterogeneity, the individual HCCs differed largely in their vulnerability against pharmacological treatment with metformin. Taken together, our approach provided a comprehensive and quantitative characterization of HCC metabolism that may pave the way for a computational *a priori* assessment of pharmacological therapies targeting metabolic processes of HCC.

Abbreviations
HCC, hepatocellular carcinoma; MMP, mitochondrial membrane potential; STAT3, signal transducer and activator of transcription 3.

Introduction

Hepatocellular carcinoma (HCC) represents the fifth most common cancer and the third most common cause of cancer-related deaths in the world [1]. The incidence of HCC in Europe and the United States is constantly rising, turning HCC into a pivotal threat to general health. Robust therapy resistance and very poor prognosis characterize HCC. Most cases of HCC develop on a pre-existing chronic liver disease, but between 15% and 50% of HCCs develop in the absence of a known etiology of liver disease, and different lines of evidence identify nonalcoholic fatty liver disease as a possible relevant risk factor for HCC [2].

The transformation of a normal liver cell (hepatocyte) to a tumor cell is accompanied by alterations of the cellular metabolism [3]. A well-known hallmark of this metabolic reprogramming is the Warburg effect characterized by a marked increase in glucose consumption and lactate formation despite the availability of oxygen. Changes in the expression level, isoform pattern, and phosphorylation status of several glycolytic enzymes contribute to the Warburg effect [4]. The functional importance of enhanced glycolytic rates for growth progression of transformed liver cells was first observed in a rodent hepatoma model [5]. In parallel, the rate of oxidative phosphorylation may be reduced or remains unchanged. It was Otto Warburg himself who reported in a seminal publication [6] that both glycolysis and respiration were significantly enhanced in transplanted tumors of Flexner–Jobling's rat carcinoma or Jensen's rat sarcoma. Later, based on experiments with Ascites tumor cells, he stated that tumor growth would result from the combination of defective mitochondria and enhanced glycolysis [7,8].

Today, we know that there are not only differences in the gene expression profiles of normal and malignant cells/tissue but also among individual tumors of the same clinical type [9,10] and even between cells in different spatial regions of a solid tumor [11]. Regarding the metabolic consequences of this heterogeneity, studies in human melanoma have provided first evidence that the metabolic program in subgroups of tumors can be either glycolytic or oxidative, depending on the expression level of PGC1α, the master regulator of mitochondrial biogenesis [12]. This finding highlights the importance of environmental factors, such as the nutritional status or the presence of pro-inflammatory immune cells, influencing the expression level of PGC1α. More general, it appears that there is not only one metabolic map of cancer but several [13]. This fact excludes a one-fits-all concept for an efficient pharmacological treatment as the 'metabolic Achilles heel' of the tumor may vary from one HCC patient to the other.

Despite the large progress achieved in the elucidation of intra- and intertumor heterogeneity in the expression of metabolic enzymes and transcription factors, a comprehensive, quantitative assessment of the functional implications of this heterogeneity is missing so far. Most studies in the field inferred tumor-specific metabolic changes from gene expression data by means of biostatistical methods of network analysis, such as pathway enrichment analysis or flux balance analysis [14]. However, the capacity of metabolic pathways is controlled not only by enzyme abundances but also by other modes of enzyme regulation, such as allosteric regulation or reversible hormone-controlled chemical modifications [15]. Often, enzymes resident in opposing pathways (e.g., synthesis and degradation of glycogen) are concomitantly up- or downregulated making it difficult to assess the net metabolic effect. Therefore, inferring metabolic changes from gene expression changes in a more reliable way calls for the use of physiology-based models, which take into account all relevant modes of metabolic regulation.

In this work, we extend our approach applied in a previous study on the heterogeneity of lipid metabolism in human HCC [16] to study a larger panel of metabolic functions in HCC. The core of our approach consists in mapping mass spectrometry resolved protein abundances of metabolic enzymes and transporters onto Hepatokin1, a kinetic model of the hepatic central metabolism [17]. We used the model to simulate the metabolic response of HCC to varying concentrations of nutrients and hormones in the blood. Applying this approach to 10 individual human HCCs revealed a large heterogeneity in the alteration of metabolic functions. Taking the usage of the anticancer drug metformin as example, we demonstrated how the knowledge of the metabolic signature of a tumor could be exploited to assess the efficacy of a pharmacological tumor therapy.

Results

Histological characterization of tissue samples

All tumors were of low or moderate extension (T1–T2). Except for one case, there was no tumor invasion into the lymph nodes or vein. The degree of fibrosis in the tumor-surrounding tissue varied largely from the absence of fibrosis (F = 0) to cirrhosis (F = 4). For detailed information, see Table 1.

Protein intensity profiles of tumors and noncancerous tissue

First, we compared protein intensity profiles (defined through label-free intensities, see Methods) of 10 HCCs (T1–T10) and their noncancerous adjacent tissue (C1–C10). In total, the proteomics yielded signals for 6502 protein-identifying peptides. From this total set, we selected a subset of 347 protein intensities, which correspond to enzymes and transporters occurring in the 174 processes contained in the metabolic model. Average network coverage, that is, the percentage of enzymes and transporters for which a protein intensity value was available from the proteomics analysis, was 84.7%.

Pearson's correlation coefficients shown in Fig. 1A revealed consistently high correlations among the protein intensity profiles of the noncancerous tissue samples (mean $R = 0.95$), irrespective of varying degrees of fibrosis of the tumor-adjacent tissue. The correlation coefficients among the protein intensity profiles of the tumors were generally lower (mean $R = 0.67$) and displayed a larger variability compared to the control tissue. Thus, potential metabolic deviations of the noncancerous tissue from normal liver tissue should be rather uniform and small compared to metabolic differences among the tumors.

The volcano plot in Fig. 1B illustrates the difference between the mean protein intensities of controls and tumors. A substantial portion of proteins (59.7%) was downregulated in the tumor, but only few enzymes were significantly upregulated. Among these proteins were subunits of the pyruvate dehydrogenase, the central enzyme enabling the transfer of carbons from glucose, pyruvate, and lactate into the citric acid cycle and ATP citrate synthase Pathways enriched in downregulated enzymes were gluconeogenesis, ketogenesis, fatty acid de novo synthesis, β-oxidation, and urea synthesis.

Metabolic signatures of individual HCCs

We defined the metabolic signature of the various tissue samples (control and tumors) by the set of the 24-h mean values of 18 different metabolic functions (for the numerical values and statistically significance of differences, see Fig. 2). Overall, eight metabolic functions were significantly downregulated but only two metabolic functions (glutamine release and β-oxidation) were upregulated in the tumors compared with the control. This finding corresponds well to the much higher number of downregulated model proteins shown in Fig. 1B. All tumors exhibited a downregulated glucose release and, except HCC3, also reduced oxygen consumption. Notably, only one tumor, HCC8, showed the characteristic features of the Warburg effect: increased glucose uptake paralleled with decreased oxygen consumption and increased lactate release.

Synthesis of urea was significantly reduced in all tumors, but ammonia detoxification was not altered due to the increased conversion of ammonia to glutamine. The largest heterogeneity with coefficients of variation larger than unity was obtained for the uptake of glucose, the uptake and release of lactate, and the size of the glycogen store.

For a better overview of metabolic similarities between the tumors and between the tumors and the control, we normalized the metabolic signatures by scaling each metabolic function to the range [0,1] with '0' corresponding the smallest and '1' corresponding to

Table 1. Characteristics of tumors and adjacent noncancerous tissues. HCCs were classified according to the tumor–nodes—metastasis classification system of malignant tumors [18]. T(0–4)—tumor size; N(0–3)—spread to regional lymph nodes; G(1–4)—differentiation grade; L (0–1)—invasion into lymphatic vessels; V(0–2)—invasion into vein; R(0–2)—completeness of the operation (resection boundaries free of cancer cells or not); LiMAx—score of the LiMAx functional liver breath test [19]. The degree of fibrosis F(0–3) and the presence of cirrhosis (F4) in the adjacent noncancerous tissue were assessed according to the Desmet and Scheuer scoring system [20].

HCC#	Gender	Age	BMI	MELD	LiMAx	T	G	L	V	R	F	Underlying liver disease
1	f	70	40.3	NA	NA	2	2	0	1	0	4	Alcohol-induced liver cirrhosis
2	m	68	27.7	6.43	498	2	2	0	1	0	2	Cryptogenic fibrosis[a]
3	m	80	27.1	9.63	469	1	3	0	0	0	1	Alcohol-induced hepatic fibrosis
4	f	22	21.0	NA	NA	1	1	0	0	0	0	No history of a chronic liver disease
5	f	67	31.2	NA	296	1a	2	0	0	0	4	Cryptogenic cirrhosis[a]
6	m	73	32.9	6.98	309	2	2	0	0	0	4	Alcohol-induced hepatic cirrhosis
7	m	71	27.3	8.00	160	2	2	0	0	0	3	Alcohol-induced advanced fibrosis
8	f	66	27.4	8.39	107	1b	2	0	0	0	4	NASH cirrhosis
9	f	59	23.0	6.43	682	2	2	0	0	0	2	Cryptogenic fibrosis[a]
10	m	77	33.8	7.92	217	1b	3	0	0	0	2	Cryptogenic fibrosis[a]

[a]The underlying etiology remains unknown as no liver disease was previously diagnosed.

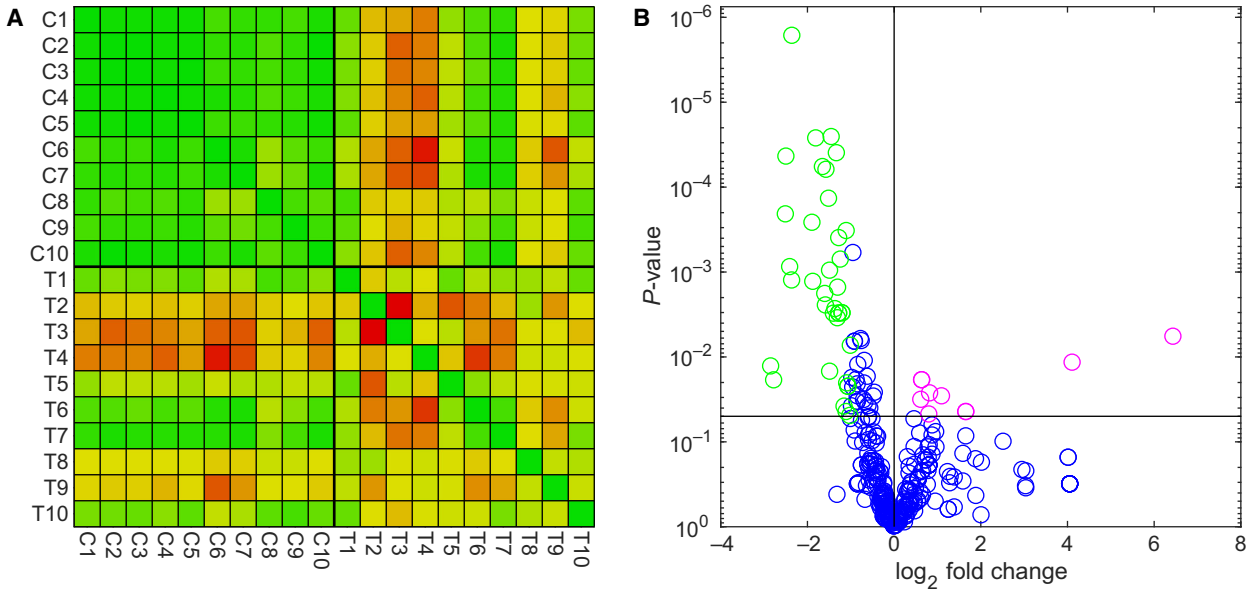

C

Upregulated	*NDUFA4L2; ACSL4; TKT; NME1; ACLY; PPA1; SLC27A3; DLAT*
Downregulated	*ENO3; GLS2; ACACB; GPT; PEPCK1; ADH4; GYS2; FBP2; ADH6; CPS1; SLC25A20; PEPCK2; ASS1; FBP1; ACADS; GLYCTK; SLC27A5; ACSL1; GPD1; MTTP; PYGL; BDH1; ADH1B; ALDOB; ACAA2; PGM1; ALDH2; GYS; ACAT2; MUT; TKFC; HMGCS2; PC; GOT1*

Fig. 1. Protein intensity profiles in tumors and controls. (A) Color-coded correlation coefficients (Pearson) among the protein intensity profiles of the 347 proteins included in the metabolic model. HCC: T1–T10; adjacent noncancerous tissue: C1–C10. (B) Fold change of the mean intensity profiles of tumors (T1–T10) over related controls (C1–C10) and statistical significance of differences assessed by means of a 2-sample *t*-test. Only protein profiles with a minimum of seven observations in both groups have been included in the analysis. (C) Upregulated enzymes (2log (fold change) > 0.5): pink dots; downregulated enzymes (2log (fold change) < −1): green dots.

the largest function value. We used Pearson's correlation coefficient to quantify the similarity between the normalized metabolic signatures of tumors and control.

None of the tumors had a metabolic signature that resembled the metabolic signature of the control with statistical significance. Arranging the tumors and the control as well as the metabolic functions based on pairwise similarities underscored the large metabolic heterogeneity (Fig. 3).

We used the overall dissimilarity between control and tumor to evaluate the extent of metabolic reprogramming present in a specific HCC. The metabolic distance between the normal hepatocyte and the tumor was defined by $D = (1 - R_{CT})/2$ where R_{CT} is Pearson's correlation coefficient quantifying the similarity between the metabolic signatures of the control and the tumor.

We identified four metabolic functions showing a statistically significant trend with increasing metabolic distance: Glucose release decreased, while fatty acid uptake, ketone body release, and β-oxidation increased with increasing metabolic distance (see Fig. 4). Hence, the values of these four metabolic 'marker' functions may indicate how far the metabolic program in a given HCC differs from that of the normal liver. However, for the majority of metabolic functions no clear trend was discernible. For example, TAG synthesis was almost identical (17.2 and 15.9 $\mu mol \cdot g^{-1} \cdot h^{-1}$) in the metabolically most distant tumors HCC4 and HCC6. Hence, our analysis gave no indication for the existence of a metabolic master program.

Finally, we analyzed whether similar gene expression profiles of tumors imply similarity of their metabolic signatures. To this end, we plotted the proteomic distance between tumors, that is, the dissimilarity of their protein intensity profiles, against the metabolic distance (see Fig. 5). Overall, the correlation was statistically insignificant ($R = 0.03$), indicating that the metabolic similarity of tumors cannot be inferred from the overall similarity of their protein expression profiles. This suggests that the regulation of metabolism by variable gene expression is not democratic but oligarchic: Differential expression of few central

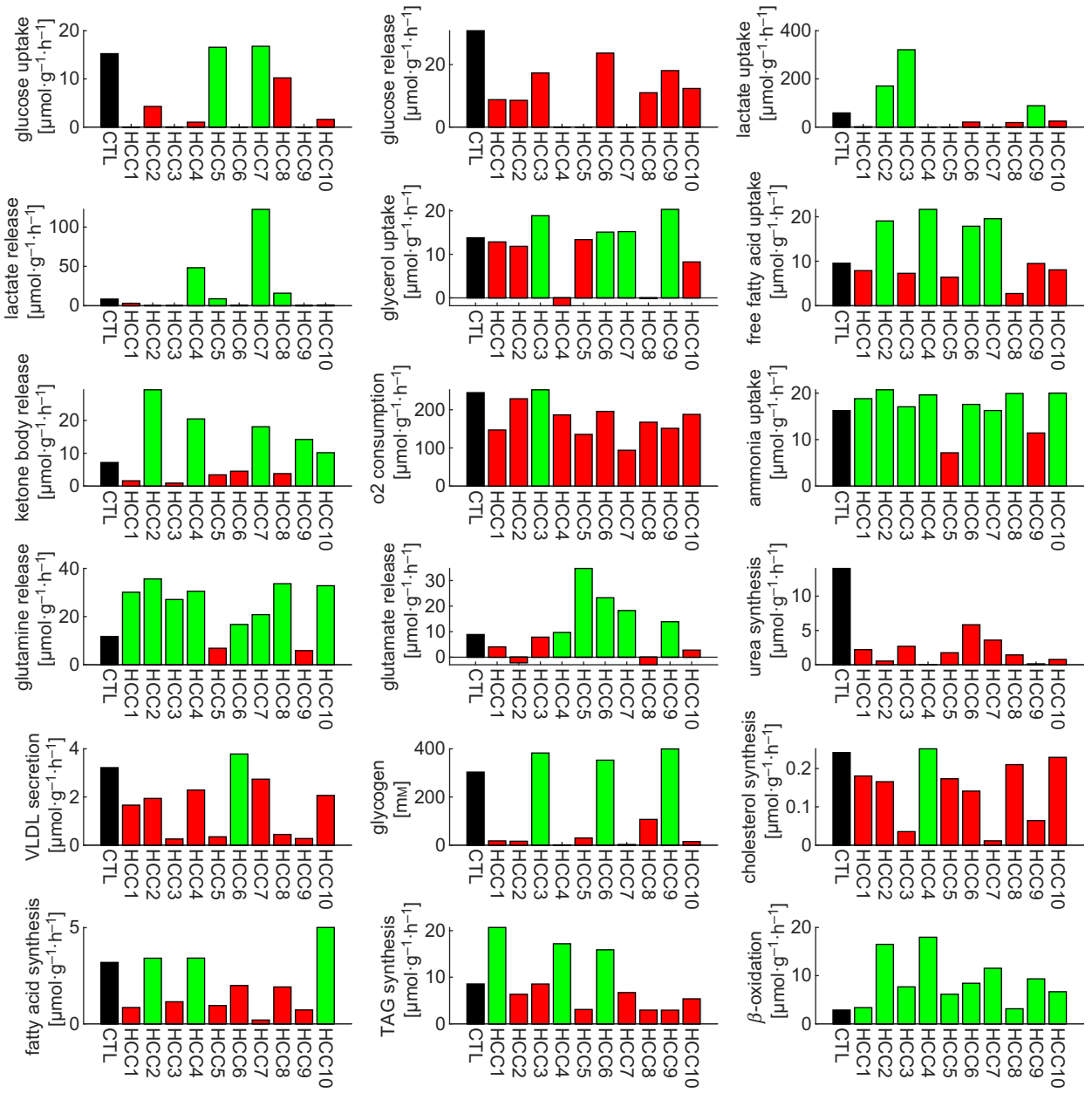

Fig. 2. Metabolic signatures of the control and tumors. The height of the bars represents the diurnal mean value of selected metabolic functions for the control (black bars) and the HCCs. Red and green bars indicate values lower or higher than those of the control.

regulatory enzymes is sufficient to imply functional dissimilarity despite large similarity in the expression of the majority of proteins [21].

Effect of metformin treatment on energy metabolism of human HCC

Effective cancer treatment should selectively damage cancerous cells while sparing the healthy surrounding tissue. The differences between the metabolism of HCC and the normal liver parenchyma give rise to the hope that metabolic enzymes could be a promising target for a selective anticancer therapy. Metformin, an antidiabetic drug, has been shown to inhibit cancer growth [22]. Metformin has at least two dose-dependent effects on central hepatic metabolism. At low concentrations, it inhibits the glycerol-3-phosphate dehydrogenase, an enzyme important for cellular redox

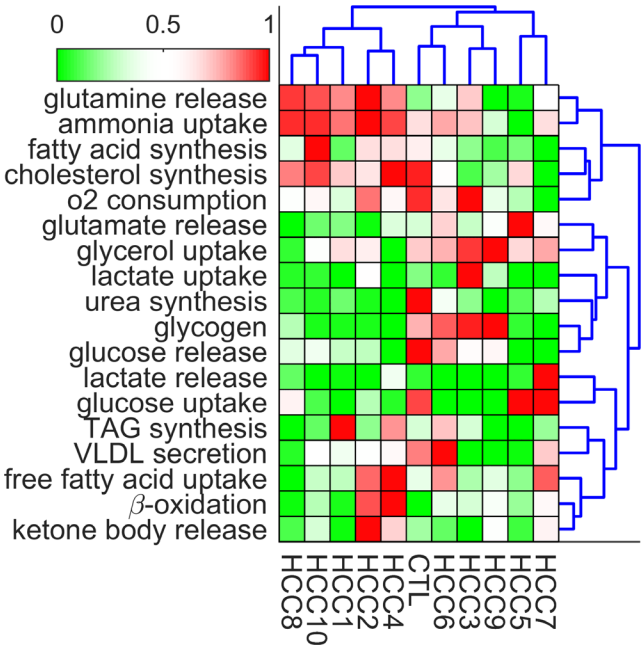

Fig. 3. Heatmap of metabolic signatures of the control and tumors. Normalized values (0: minimal value; 1: maximal value) of selected metabolic functions (rows) for tumors and control (columns) are represented by different colors (green: low values; red: high values). Both columns and rows were arranged in the order of hierarchical clusters based on Ward's method.

balance by shuttling electrons from the cytosol to the respiratory chain. This effect is supposed to be responsible for the antidiabetic effect [23]. At higher concentrations, metformin is a potent inhibitor of complex I of the respiratory chain [22]. We simulated the effect of increasing plasma concentrations of metformin on cellular viability for healthy hepatocytes and the different HCCs.

We simulated the effect of metformin on the energy metabolism of HCC and control (see Fig. 6) using the reported inhibition constants of 0.5 mM for complex I [22] and 0.055 mM for glycerol-3-phosphate dehydrogenase [23]. Increasing metformin concentration led to a rise of the mitochondrial membrane potential (MMP) and drop of the ATP level and the oxygen uptake rate. It is known that an increase in the MMP to values above −80 mV contributes to the formation of a permeability transition pore that enables the efflux of cytochrome *c*, an initial event in the induction of apoptosis [24,25]. For normal hepatocytes, this threshold is reached at a critical metformin concentration of about 0.8 mM. For the individual HCC, this critical concentration varied largely. HCC9 was predicted to be most sensitive to metformin treatment, reaching the apoptotic threshold already at 0.2 mM metformin. On the other hand, for five HCCs an effective treatment with metformin should not be possible without exerting significant side effects for the normal liver parenchyma. Of note, vulnerability of tumors to metformin did not correlate with metabolic distance to the control. In summary, the simulations predicted metformin to be a selective anticancer drug for four out of the 10 HCCs.

Discussion

A personalized systems biology approach to the characterization of tumor metabolism

A key challenge in cancer research is to establish methods that reliably report the metabolic features of intact tumors, particularly in patients. Techniques to measure metabolic functions *in vivo* are rare [26]. Estimating fluxes *in vivo* by measuring time series of labeled nutrients [27] is restricted to the analysis of very few pathways and not suited for monitoring metabolic fluxes over a longer period of varying physical activity and plasma profiles of nutrients. Therefore, we developed a novel approach that combines proteomic analysis of liver tissue with kinetic modeling of liver metabolism. In a preceding work [28], we demonstrated that this approach is capable of correctly predicting the metabolic phenotype of liver tumors in a mouse model. In this work, we used proteomics data on protein

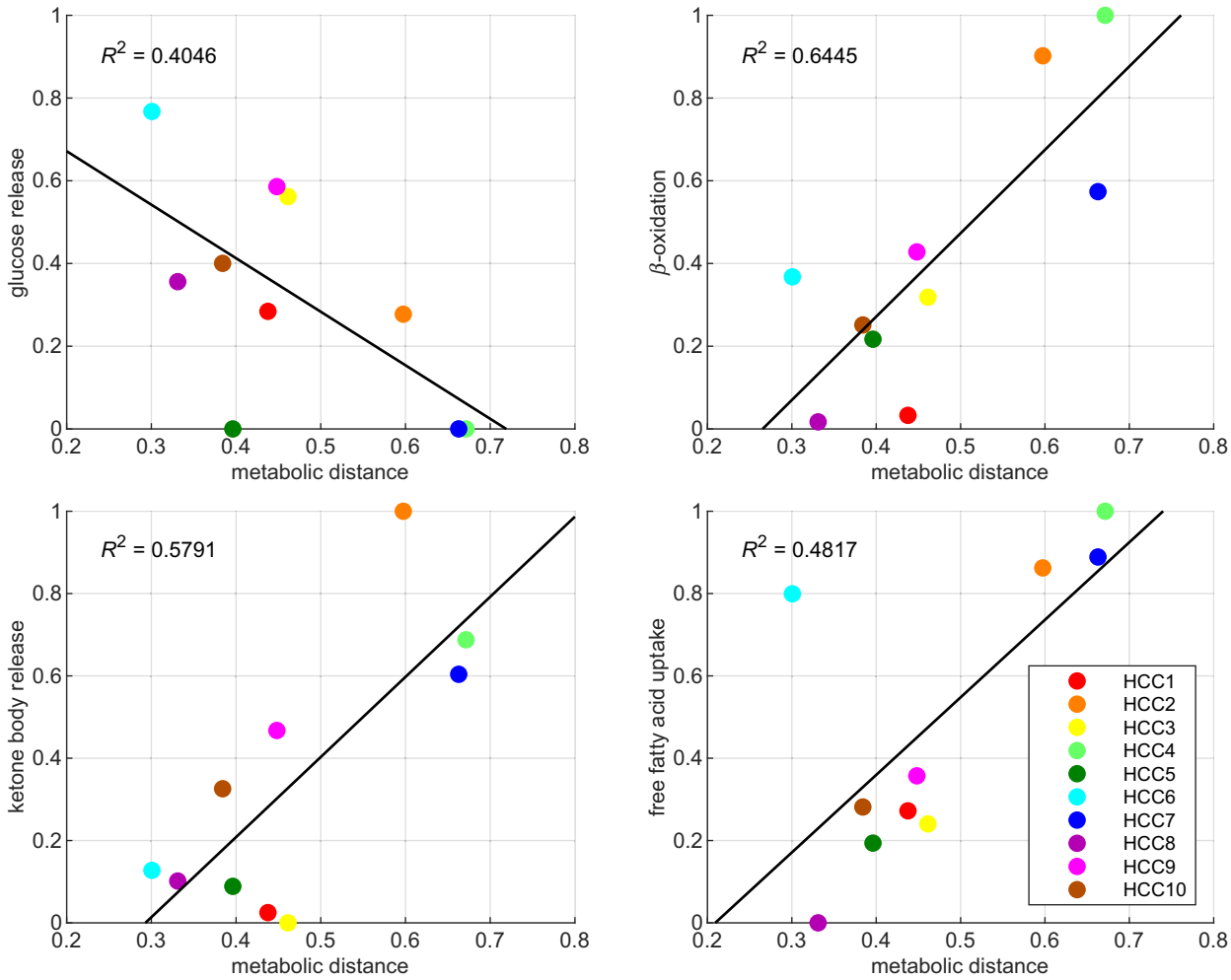

Fig. 4. Metabolic functions displaying a significant trend with increasing metabolic distance between control and tumor. Values of metabolic functions are given in relative units (0: smallest value; 1: largest value). The metabolic distance between control and tumor is measured by $D = (1 - R_{CT})/2$ with R_{CT} being Pearson's correlation coefficient of their relative metabolic functions. Linear regression trend lines are shown with the coefficients of determination R^2 given. Correlations are significant with *P*-values of $P = 0.048$ (glucose release), $P = 0.005$ (β-oxidation), $P = 0.011$ (ketone body release), and $P = 0.026$ (fatty acid uptake).

abundances in human HCC and the surrounding liver tissue to construct tumor-specific metabolic models allowing us to monitor a larger panel of metabolites and fluxes in response to a typical plasma profile of metabolites and hormones.

Metabolic heterogeneity of individual HCCs

Our results revealed large variations of metabolic capacities in individual HCCs. Possible reasons for this heterogeneity may lie in the tissue environment of the tumor [29], different mutation patterns in key signaling pathways [30], and intratumor zonation arising from regional hypoxia due to diffusion limitations in combination with altered and nonfunctional tumor microvasculature [31,32]. The resulting metabolic zonation may promote the growth capacity of tumors [33].

Although with considerable quantitative differences, some metabolic functions deviated consistently from those of the surrounding tissue. Both glycolysis and gluconeogenesis were found to be downregulated in all HCCs, while there was a clear trend toward increased uptake and β-oxidation of free fatty acids. Urea synthesis was also lowered in all tumors, paralleled by an increase of ammonia fixation in glutamine. As glycolysis and urea synthesis represent ATP-consuming pathways that the liver runs for the benefit of the organism and not of its own, downregulation of these pathways would save a lot of ATP that the tumor can favorably spend on its biomass production.

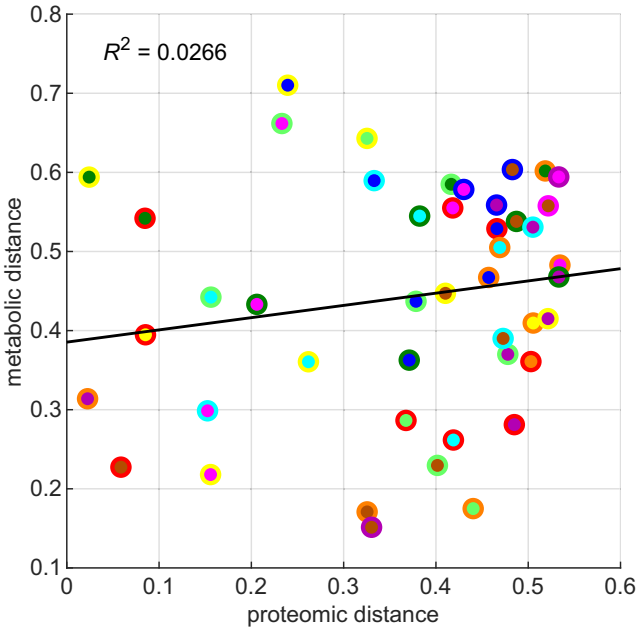

Fig. 5. Metabolic distance of tumors versus proteomic distance. Metabolic distances between all pairs of tumors are shown against their proteomic distance. The proteomic distance between two tumors is defined by $D = (1 - R_{TT})/2$ with R_{TT} being Pearson's correlation coefficient of their metabolic gene expression profiles (see Table S1). There is no statistical significant correlation between metabolic and proteomic distance in general. A linear regression trend line is shown with the coefficient of determination R^2 given.

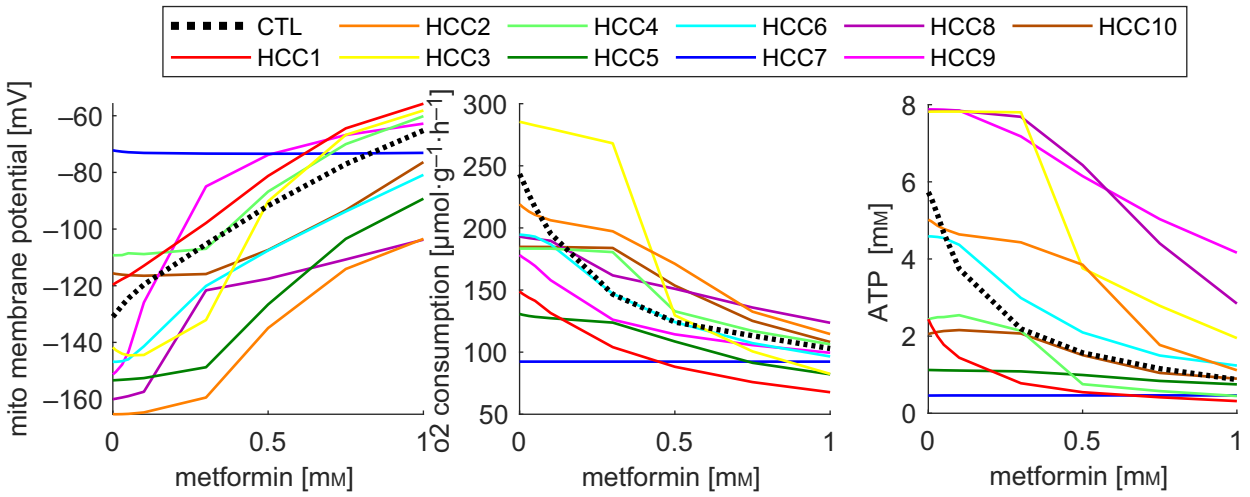

Fig. 6. Effect of metformin on the MMP, oxygen consumption rate, and cellular ATP level in healthy liver (black dotted line) and 10 human HCCs. We fixed the external conditions by putting the plasma nutrient concentrations to their mean diurnal values and using the corresponding plasma hormone concentrations. The threshold value of the MMP above which apoptosis is initiated was set to −75 mV.

Importantly, only one HCC had the classical features of the Warburg effect, which is commonly considered to dominate metabolic reprogramming of HCC [34]. This discrepancy might be due to the fact that the metabolism of HCC can be shaped by the availability of nutrients [29]. In an inflammatory and steatotic environment, a high fatty acid load may force HCC to become more reliant on fatty acids as an energy source.

Therefore, *in vitro* findings with isolated tumor cells bathing in a medium that is rich in glucose but does not contain free fatty acids bear the risk of inadequately reflecting the *in vivo* situation. Furthermore, evidences for the presence of the Warburg effect in HCC often rely on transcriptomic data of selected enzymes or transcription factors known to control the capacity of glycolysis and oxidative phosphorylation. Such studies notoriously overlook the fact that variable gene expression is only one mode of cellular regulation among a multitude of other regulatory mechanisms that together determine the metabolic phenotype [15]. This is convincingly demonstrated by the capability of the liver to switch from glucose uptake to glucose production without changing the expression of a single enzyme. Anyway, despite the small number of tumors included, our study suggests that realization of the Warburg type should be ruled out as a general principle governing metabolic reprogramming of HCC.

Carbohydrate metabolism

Suppression of gluconeogenesis in HCC has been accounted for by signal transducer and activator of transcription 3 (STAT3)-mediated activation of microRNA-23a [35]. Interleukin 6-induced activation of STAT3 is a typical response of the liver to inflammation [36]. Hence, the level of STAT3 activation and the suppression level of STAT3 may depend on whether the tumor growth proceeds in an inflammatory environment or not. Lower expression of fructose-1,6-bisphosphatase, the rate-limiting enzyme in gluconeogenesis, was associated with advanced tumor stage, poor overall survival, and higher tumor recurrence rates [37]. Of note, the reduction of gluconeogenesis was one of the leading metabolic features that correlated well with the metabolic distance between control and tumor (see Fig. 4A). Hence, it is tempting to speculate that the metabolic distance between tumor and hepatocyte delivered by our approach may help to evaluate the malignant potential of a given HCC.

The glycogen store was one of the metabolic parameters showing the largest variability among the 10 tumors. Glycogen has a crucial role to promote cell survival under hypoxic conditions in normal and cancer cells [38]. Lea *et al.* [39] reported that glycogen metabolism in slowly growing hepatoma resembles more closely that in normal rat liver than does glycogen metabolism in rapidly growing hepatoma in which glycogen levels were very low. In our study, tumors with the lowest glycogen store (HCC2, HCC4, and HCC7) were those having the largest metabolic distance to the normal hepatocyte. This observation lends further support to the presumption that the malignant potential of HCC correlates with increasing metabolic distance from the normal hepatocyte. It has to be noted, however, that studies with different tumor cell lines of hepatocellular origin did not show distinct correlation between the degree of tumor cell dedifferentiation and their ability to accumulate glycogen [40]. A high glycolytic capacity and the ability to store large amount of glycogen are often viewed as adaptation to hypoxic conditions, but the correlation between glucose uptake rates and glycogen content was insignificant ($R^2 = 0.073$) in our study.

Lipid metabolism

Our analysis revealed a trend of HCC to increase the uptake of free fatty acids as energy-delivering substrates. It has been shown that a subclass of HCC carrying activating mutations in *CTNNB1*, encoding β-catenin, is addicted to fatty acids [41]. In a mouse model (Apc^{TumLIV} mouse) mimicking *CTNNB1*-mutated HCC tumorigenesis, the tumor had normal glucose and lactate metabolism but a high rate of fatty acid β-oxidation, which was correlated with increased synthesis of ketone bodies and reduced fatty acid esterification in triacylglycerols. Our data also revealed a significant positive correlation between β-oxidation and ketone body formation (see Fig. 4), but the glucose metabolism was generally downregulated. Possibly, the mouse model reflects only in part the metabolic features of human HCC *in vivo*, which may also be deregulated in several other signaling pathways (RAS/ERK, P13K/AKT, IKK/NF-κB, TGF-β, NOTCH, Hedgehog, and Hippo).

Several reports in the literature have indicated the relevance of fatty acid synthesis in HCC [42–44]. Immunohistochemical staining showed that the key regulatory enzyme, the fatty acid synthase, was positively expressed in all 20 HCC patients studied, whereas the positive expression rate in tumor-adjacent tissue was only 10% [43]. Notably, upregulation of fatty acid synthesis and upregulation of β-oxidation are not mutually exclusive in tumors [45]. In our study, three tumors (2, 4, and 10) exhibited concomitant upregulation of these two opposing pathways (see Fig. 2).

Calvisi *et al.* [42] concluded from their study of human HCC that transformation of normal liver tissue to precancerous tissue and ultimately HCC is accompanied by a steady upregulation of prolipogenic enzymes and increased accumulation of cholesterol and TAG, irrespective of the etiology of HCC. Averaged across all 10 HCC, our protein expression data

do not confirm this finding. However, for a subset of three HCC, we found significantly elevated levels of TAG. In the publication by Calvisi *et al.* [42], the by far highest activation of lipogenesis was observed in HCC with poor prognosis (survival < 3 years) whereas the differences of TAG and cholesterol in the tumor-surrounding tissue and HCC with better prognosis were marginal as in our study.

Finally, cholesterol synthesis was found to be significantly reduced in nine HCCs. Downregulation of cholesterol synthesis may be another strategy of HCC to promote tumor progression by reducing the formation of cholesterol-enriched lipid rafts in the plasma membrane. CD44, a protein crucial for cell migration and cancer metastasis, is preferentially located in such lipid rafts. High extracellular levels of cholesterol have been demonstrated to effectively reduce the activity of CD44 and thus HCC migration and invasion [46].

Ammonia/amino acid metabolism

In the healthy liver, ammonia detoxification is divided into urea formation (preferentially in periportal hepatocytes) and glutamine/glutamate synthesis (preferentially in pericentral hepatocytes). Our simulations revealed that rate of urea synthesis was downregulated in all HCCs because of downregulation of the carbamoyl phosphate synthetase 1. Liu *et al.* [47] showed that the drastically lowered expression of carbamoyl phosphate synthetase 1 in HCC results from DNA hypermethylation near the transcription start site of the corresponding gene. Intriguingly, in eight HCCs, the uptake rate of ammonia was not lowered because the reduced conversion of ammonia to urea was compensated by an increased rate of glutamine synthesis. In the normal liver, glutamine synthetase expression is restricted to pericentral hepatocytes, but in adenoma-like neoplasms and in HCC, a strong and diffuse glutamine synthetase expression was seen. Glypican3, a regulatory protein involved in Wnt signaling, is associated with glutamine synthetase expression, and glypican3 immunopositivity is a highly specific and sensitive indicator for HCC [48]. As glutamine is one of the major energy and nitrogen sources of tumor cells, it is tempting to speculate that redirecting the fixation of ammonia from urea synthesis to glutamine synthesis is a strategy of HCC to increase the abundance of this important carbon and nitrogen source.

Energy metabolism as target of anticancer drugs

Except HCC3, all HCCs displayed a stable MMP below −100 mV, a value that is clearly below the critical value of about −80 mV where opening of the mitochondrial transition pore may start. Six HCCs had an even more negative MMP than the normal hepatocyte. The MMP is a crucial model parameter because it largely determines the sensitivity of HCC to mitochondrial inhibitors such as corilagin, a natural plant polyphenol belonging to the class of hydrolyzable tannins, that may induce apoptosis of HCC by effectively depolarizing the MMP [49]. Our simulations suggested that four HCCs might be particularly susceptible to metformin-induced energy impairment.

Limitations of our approach

The most difficult problem in studying metabolic differences between normal and diseased human tissue is the definition of the 'normal' control. In this work, we equated the protein intensity profiles of the tumor-adjacent tissue with 'normal' enzyme activities of a generic healthy liver [17], thereby neglecting individual deviations from this generic reference state. Some justification of this setting comes from the persistently high correlation of protein intensity profiles among nontumorous liver samples (see Fig. 1A). Another issue is the incomplete network coverage with protein data. For gap filling, we applied an imputation method that rests on the plausible but debatable assumption that proteins with measured, strongly correlating expression levels in a subset of tumors should also have similar expression levels in tumors for which experimental data are not available. Given the sometimes erratic expression changes in malignant cells due to the high number of metabolism-related mutations, this assumption may fail and improvement of the proteomics analysis as well as more appropriate gap-filling methods is needed. A third problem is the definition of boundary conditions for an individual tumor. In our approach, we confronted all tumors with the same 24-h plasma profile of metabolites and hormones. If it would be possible in future studies to monitor the plasma profile of individual patients, these could be used as patient-specific model input. It also has to be noted that our model simulations were performed with unaltered hormonal signaling pathways that are responsible for the interconversion of metabolic enzymes. While the first three issues lie in the limited data quality available for human patients, it remains a future task to extend the metabolic model by a more detailed kinetic model of hormone-dependent signaling that is amenable to tumor-specific parametrization.

Finally, it has to be emphasized that the findings of our study must be taken cautiously given the small

number of patients included. Application of our approach to a much larger number of tumors will be needed to arrive at a reliable assessment of the probability with which a specific metabolic subtype of HCC may occur at a given stage of development and known driver mutations and etiology of the underlying liver disease.

Conclusion

Taken together, our study revealed a large heterogeneity of metabolic changes in HCC, which do not follow a single 'master program' but instead may result from a plethora of simultaneously operative influencing factors, such as the availability and quality of nutrients, the medication history of the patient, comorbidities (e.g., diabetes), random mutations in proteins of regulatory pathways, metabolic responses to virus load, humoral signals received from inflammatory immune cells, cell–cell and cell–matrix contacts, and the extension and differentiation of the tumor. This situation calls for personalized treatment options that are based on a careful analysis of the tumor-specific metabolic capabilities. Our approach may serve as a promising step in this direction.

Materials and methods

Major parts of the following methods have also been described in an earlier publication [16].

Outline of the approach

We combined experimentally determined protein abundance profiles of metabolic enzymes and membrane transporters with kinetic modeling of liver metabolism (see Fig. 7).

Hepatocellular carcinoma tissue and adjacent noncancerous tissue were taken from patients undergoing curative liver resection. Label-free LC-MS/MS shotgun proteomics was used to generate quantitative protein intensity profiles of the paired tissue samples.

The maximal activity of an enzyme (v_{max}) is related to the protein concentration (E) by

$$v_{max} = k_{cat} E, \tag{1}$$

where k_{cat} is the catalytic rate constant (or turnover number) of the enzyme/transporter. The shotgun proteomics yields only the protein intensity (E') which depends on the flight behavior of the peptides used as protein identifiers. Hence, the protein intensity is related to the absolute protein concentration by an unknown factor γ,

$$E = \gamma E'. \tag{2}$$

If the maximal activity v_{max}^{ref} is already known for a reference state of the metabolic system, then the v_{max} value of another metabolic state (here the metabolic state of the tumor) can be calculated by exploiting the relations (1) and (2):

$$v_{max}^{tumor} = v_{max}^{ref} \frac{E'^{tumor}}{E'^{ref}}. \tag{3}$$

Usage of relation (3) circumvents the problem of converting the protein intensities to absolute protein abundances. The vector constituted by the ratios E'^{tumor}/E'^{ref} of enzyme intensities defines the *enzyme expression signature* of the tissue under investigation (see Table S1).

The tumor-specific maximal activities defined in (3) were used in Hepatokin1, a kinetic model of central liver metabolism comprising the main pathways of energy, carbohydrate, lipid, and amino acid metabolism [17]. The model simulations were performed by using a typical 24-h plasma profile of hormones and exchangeable metabolites as model input [17]. The protein intensities of the noncancerous tissue adjacent to the tumor were treated as representing the proteome of normal liver tissue associated with the v_{max} values used in the generic model for the healthy liver (for the estimation of v_{max}^{ref}, see [17]).

The abundance of model proteins with lacking protein intensities was estimated by means of a statistical imputation method used in Ref. [16]. In brief, we compiled a list of reference proteins, for which measured intensities were available for all 10 controls and 10 tumors. For each model protein with missing protein intensity value in a given tumor, we determined all reference proteins exhibiting a Spearman correlation larger than a critical threshold value $R_{crit} = 0.8$. Linear regression analysis with each of these highly correlating reference proteins yielded a group of estimates for the missing value. The group mean was then used as substitute for the missing protein intensity.

Acquisition of tissue samples

Hepatocellular carcinoma tissues and adjacent noncancerous tissues were collected from 10 patients, which underwent curative resection (R0) at the Department of Surgery of the Charité. Ethical approval for tissue sampling and analysis was obtained from the ethics committee at Charité —Universitätsmedizin Berlin (EA1/140/15). The patients gave informed consent in writing and in accordance with the declaration of Helsinki to the scientific use of their resected tissue specimen for molecular analyses. Macroscopically, the analyzed HCC tissues were graded according to the tumor–nodes–metastasis classification [18]. No distant metastases or spreading to lymph nodes were found.

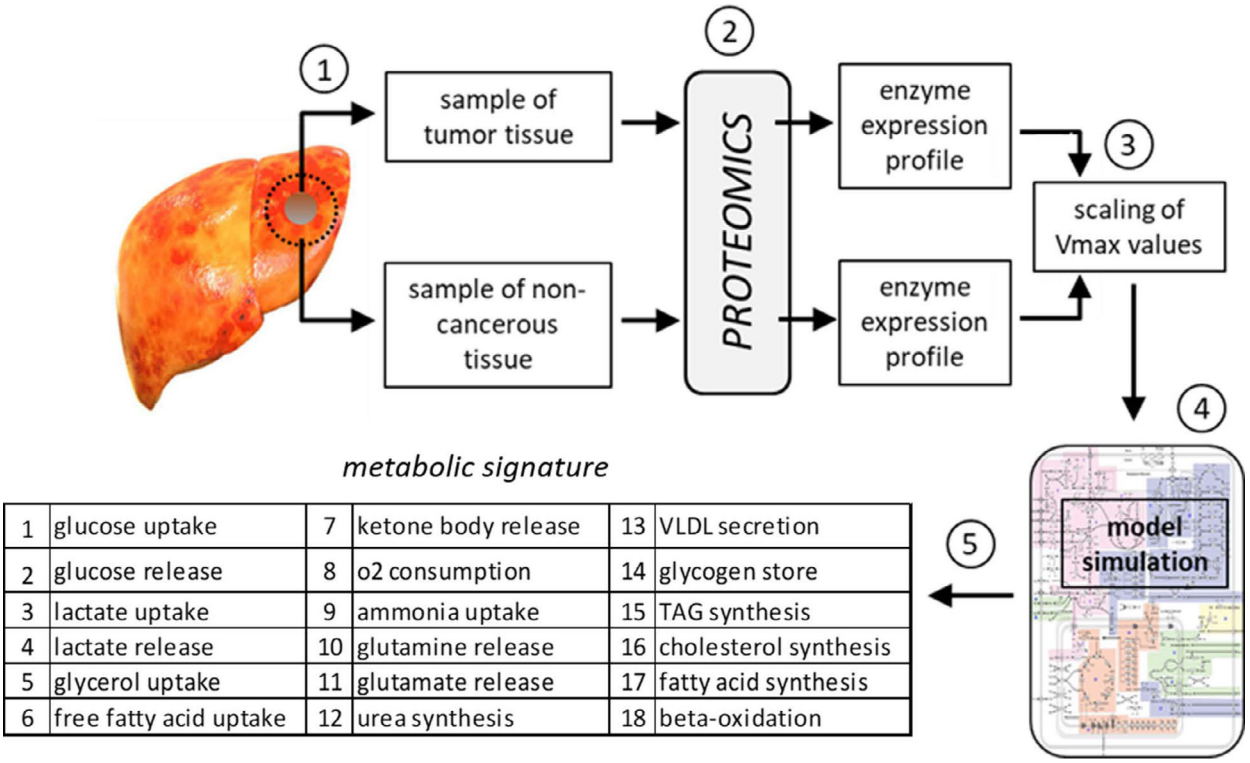

Fig. 7. Main steps in the generation of tumor-specific metabolic signatures. (1) Tissue samples from the tumor (HCC) and the tumor-surrounding noncancerous tissue (control) are taken during curative surgery. (2) Quantitative shotgun proteomics of enzymes and transporters yields protein intensity profiles. (3) Tumor-specific calibration of the kinetic model based on the difference (fold change) between the protein intensity profiles of tumor and control. (4) Model simulations over a 24-h cycle using the plasma profile of exchangeable metabolites and hormones (insulin and glucagon) as model input [17]. (5) 24-h mean values of 21 metabolic functions define the metabolic signature of the tumor.

The resected tissue was used for tumor grading according to Hamilton and Aaltonen (Eds.) (2000) [50].

Quantitative proteomics of tissue samples

Frozen liver tissue was cut into pieces of ~ 10 mg with cooled tweezers and scalpel in a precooled mortar. They were transferred into screw lid vials, which contained a precooled disruption bead and 1 mL lysis buffer. Additionally, samples were kept on dry ice to prevent thawing. To avoid proteolytic activity, tissues were homogenized immediately with a FastPrep. Tissues were homogenized under denaturing conditions with a FastPrep (three times for 60 s, 6.5 $m \cdot s^{-1}$) in a lysis buffer containing 1% sodium deoxycholate, 10 mM Tris(2-carboxyethyl)phosphine, 40 mM chloroacetamide, and 100 mM Tris, pH 8.5. The homogenates were then lysed at 95 °C for 10 min followed by 5-min sonication. The 50 µL aliquots of lysates were digested and purified using the preOmics in-Stage Tip Kit (iST Kit 96x, Martinsried, Germany). Samples were eluted sequentially in three fractions using the SDB-RPS-1 and SDB-RPS-2 buffers [51] and the elution buffer provided by preOmics for subsequent analysis on a Nano LC-MS.

LC-MS/MS was carried out by nanoflow reverse-phase liquid chromatography (Dionex Ultimate 3000; Thermo Scientific, Waltham, MA, USA) coupled online to a Q Exactive HF Orbitrap mass spectrometer (Thermo Scientific). The LC separation was performed using a PicoFrit analytical column (75 µm ID × 55 cm long, 15 µm Tip ID; New Objectives, Woburn, MA, USA) in-house packed with 3-µm C18 resin (ReproSil-Pur C18-AQ, 3 µm, Dr. Maisch, Ammerbuch-Entringen, Germany), as reported previously [52]. Briefly, peptides were eluted using a gradient from 3.8% to 50% solvent B in solvent A over 121 min at 266 $nL \cdot min^{-1}$ flow rate. Solvent A was 0.1% formic acid, and solvent B was 79.9% acetonitrile, 20% water, and 0.1% formic acid. Nanoelectrospray was generated by applying 3.5 kV. A cycle of one full Fourier transformation scan mass spectrum (300–1750 *m/z*, resolution of 60 000 at *m/z* 200, AGC target 1e6) was followed by 12 data-dependent MS/MS scans (resolution of 30 000, AGC target 5e5) with a normalized collision energy of 25 eV. In order to

avoid repeated sequencing of the same peptides, a dynamic exclusion window of 30 s was used. In addition, only the peptide charge states between two and eight were sequenced.

Raw MS data were processed with MAXQUANT software (1.5.7.4) [51] with the Andromeda search engine [53] and the human UniProtKB with 70 228 entries released in 02/2016. A false discovery rate of 0.01 for proteins and peptides, a minimum peptide length of seven amino acids, a mass tolerance of 4.5 p.p.m. for precursor, and 20 p.p.m. for fragment ions were required. A maximum of two missed cleavages was allowed for the tryptic digest. Cysteine carbamidomethylation was set as fixed modification, while N-terminal acetylation and methionine oxidation were set as variable modifications.

Acknowledgements

This research was funded by the German Systems Biology Programs 'LiSyM', grant no. 31L0057 and 031L0058, sponsored by the German Federal Ministry of Education and Research (BMBF) and the Max Planck Society. Open access funding enabled and organized by ProjektDEAL.

Conflict of interest

The authors declare no conflict of interest.

Author contributions

H-GH administered the project. H-GH and NB conceived the study. NB contributed to modeling. MS, TW, and NH participated in clinical investigation. DM and RG carried out proteomics. JE, NH, and H-GH curated the data. H-GH and NB wrote the original draft of the manuscript. DM and NH reviewed and edited the manuscript. H-GH, DM, and MS acquired funding.

References

1 El-Serag HB & Rudolph KL (2007) Hepatocellular carcinoma: epidemiology and molecular carcinogenesis. *Gastroenterology* **132**, 2557–2576.
2 Petta S & Craxi A (2010) Hepatocellular carcinoma and non-alcoholic fatty liver disease: from a clinical to a molecular association. *Curr Pharm Des* **16**, 741–752.
3 Geschwind JF, Georgiades CS, Ko YH & Pedersen PL (2004) Recently elucidated energy catabolism pathways provide opportunities for novel treatments in hepatocellular carcinoma. *Expert Rev Anticancer Ther* **4**, 449–457.
4 Herling A, Konig M, Bulik S & Holzhutter HG (2011) Enzymatic features of the glucose metabolism in tumor cells. *FEBS J* **278**, 2436–2459.
5 Lo CH, Farina F, Morris HP & Weinhouse S (1968) Glycolytic regulation in rat liver and hepatomas. *Adv Enzyme Regul* **6**, 453–464.
6 Warburg O, Wind F & Negelein E (1927) The metabolism of tumors in the body. *J Gen Physiol* **8**, 519–530.
7 Warburg O (1956) On respiratory impairment in cancer cells. *Science* **124**, 269–270.
8 Warburg O (1956) On the origin of cancer cells. *Science* **123**, 309–314.
9 Gentric G, Mieulet V & Mechta-Grigoriou F (2017) Heterogeneity in cancer metabolism: new concepts in an old field. *Antioxid Redox Signal* **26**, 462–485.
10 Lu LC, Hsu CH, Hsu C & Cheng AL (2016) Tumor heterogeneity in hepatocellular carcinoma: facing the challenges. *Liver Cancer* **5**, 128–138.
11 Nabi K & Le A (2018) The intratumoral heterogeneity of cancer metabolism. *Adv Exp Med Biol* **1063**, 131–145.
12 Vazquez F, Lim JH, Chim H, Bhalla K, Girnun G, Pierce K, Clish CB, Granter SR, Widlund HR, Spiegelman BM *et al.* (2013) PGC1alpha expression defines a subset of human melanoma tumors with increased mitochondrial capacity and resistance to oxidative stress. *Cancer Cell* **23**, 287–301.
13 Strickaert A, Saiselet M, Dom G, De Deken X, Dumont JE, Feron O, Sonveaux P & Maenhaut C (2017) Cancer heterogeneity is not compatible with one unique cancer cell metabolic map. *Oncogene* **36**, 2637–2642.
14 Creixell P, Reimand J, Haider S, Wu G, Shibata T, Vazquez M, Mustonen V, Gonzalez-Perez A, Pearson J, Sander C *et al.* (2015) Pathway and network analysis of cancer genomes. *Nat Methods* **12**, 615–621.
15 Bulik S, Holzhutter HG & Berndt N (2016) The relative importance of kinetic mechanisms and variable enzyme abundances for the regulation of hepatic glucose metabolism–insights from mathematical modeling. *BMC Biol* **14**, 15.
16 Berndt N, Eckstein J, Heucke N, Gajowski R, Stockmann M, Meierhofer D & Holzhutter HG (2019) Characterization of lipid and lipid droplet metabolism in human HCC. *Cells* **8**, 512.
17 Berndt N, Bulik S, Wallach I, Wunsch T, Konig M, Stockmann M, Meierhofer D & Holzhutter HG (2018) HEPATOKIN1 is a biochemistry-based model of liver metabolism for applications in medicine and pharmacology. *Nat Commun* **9**, 2386.
18 Edge SB & Compton CC (2010) The American Joint Committee on Cancer: the 7th edition of the AJCC cancer staging manual and the future of TNM. *Ann Surg Oncol* **17**, 1471–1474.

19 Stockmann M, Lock JF, Malinowski M, Niehues SM, Seehofer D, Neuhaus P. The LiMAx test: a new liver function test for predicting postoperative outcome in liver surgery. *HPB*. 2010;**12**:139–146. http://dx.doi.org/10.1111/j.1477-2574.2009.00151.x.
20 Desmet VJ, Gerber M, Hoofnagle JH, Manns M & Scheuer PJ (1994) Classification of chronic hepatitis: diagnosis, grading and staging. *Hepatology* **19**, 1513–1520.
21 Bulik S, Grimbs S, Huthmacher C, Selbig J & Holzhutter HG (2009) Kinetic hybrid models composed of mechanistic and simplified enzymatic rate laws – a promising method for speeding up the kinetic modelling of complex metabolic networks. *FEBS J* **276**, 410–424.
22 Wheaton WW, Weinberg SE, Hamanaka RB, Soberanes S, Sullivan LB, Anso E, Glasauer A, Dufour E, Mutlu GM, Budigner GS *et al*. (2014) Metformin inhibits mitochondrial complex I of cancer cells to reduce tumorigenesis. *Elife* **3**, e02242.
23 Madiraju AK, Erion DM, Rahimi Y, Zhang XM, Braddock DT, Albright RA, Prigaro BJ, Wood JL, Bhanot S, MacDonald MJ *et al*. (2014) Metformin suppresses gluconeogenesis by inhibiting mitochondrial glycerophosphate dehydrogenase. *Nature* **510**, 542–546.
24 Bonora M & Pinton P (2014) The mitochondrial permeability transition pore and cancer: molecular mechanisms involved in cell death. *Front Oncol* **4**, 302.
25 Ly JD, Grubb DR & Lawen A (2003) The mitochondrial membrane potential (deltapsi(m)) in apoptosis; an update. *Apoptosis* **8**, 115–128.
26 Beylot M, Peroni O, Diraison F & Large V (1996) New methods for in vivo studies of hepatic metabolism. *Reprod Nutr Dev* **36**, 363–373.
27 Hensley CT, Faubert B, Yuan Q, Lev-Cohain N, Jin E, Kim J, Jiang L, Ko B, Skelton R, Loudat L *et al*. (2016) Metabolic heterogeneity in human lung tumors. *Cell* **164**, 681–694.
28 Berndt N, Egners A, Mastrobuoni G, Vvedenskaya O, Fragoulis A, Dugourd A, Bulik S, Pietzke M, Bielow C, van Gassel R *et al*. (2019) Kinetic modelling of quantitative proteome data predicts metabolic reprogramming of liver cancer. *Br J Cancer* **122**, 233–244.
29 Wang H, Lu J, Dolezal J, Kulkarni S, Zhang W, Chen A, Gorka J, Mandel JA & Prochownik EV (2019) Inhibition of hepatocellular carcinoma by metabolic normalization. *PLoS One* **14**, e0218186.
30 Gao P, Tchernyshyov I, Chang TC, Lee YS, Kita K, Ochi T, Zeller KI, De Marzo AM, Van Eyk JE, Mendell JT *et al*. (2009) c-Myc suppression of miR-23a/b enhances mitochondrial glutaminase expression and glutamine metabolism. *Nature* **458**, 762–765.
31 Jain RK (2005) Normalization of tumor vasculature: an emerging concept in antiangiogenic therapy. *Science* **307**, 58–62.
32 Semenza GL (2008) Tumor metabolism: cancer cells give and take lactate. *J Clin Invest* **118**, 3835–3837.
33 Konig M, Holzhutter HG & Berndt N (2013) Metabolic gradients as key regulators in zonation of tumor energy metabolism: a tissue-scale model-based study. *Biotechnol J* **8**, 1058–1069.
34 Shang RZ, Qu SB & Wang DS (2016) Reprogramming of glucose metabolism in hepatocellular carcinoma: progress and prospects. *World J Gastroenterol* **22**, 9933–9943.
35 Wang B, Hsu SH, Frankel W, Ghoshal K & Jacob ST (2012) Stat3-mediated activation of microRNA-23a suppresses gluconeogenesis in hepatocellular carcinoma by down-regulating glucose-6-phosphatase and peroxisome proliferator-activated receptor gamma, coactivator 1 alpha. *Hepatology* **56**, 186–197.
36 He G & Karin M (2011) NF-kappaB and STAT3 – key players in liver inflammation and cancer. *Cell Res* **21**, 159–168.
37 Hirata H, Sugimachi K, Komatsu H, Ueda M, Masuda T, Uchi R, Sakimura S, Nambara S, Saito T, Shinden Y *et al*. (2016) Decreased expression of fructose-1,6-bisphosphatase associates with glucose metabolism and tumor progression in hepatocellular carcinoma. *Cancer Res* **76**, 3265–3276.
38 Favaro E, Bensaad K, Chong MG, Tennant DA, Ferguson DJ, Snell C, Steers G, Turley H, Li JL, Gunther UL *et al*. (2012) Glucose utilization via glycogen phosphorylase sustains proliferation and prevents premature senescence in cancer cells. *Cell Metab* **16**, 751–764.
39 Lea MA, Murphy P & Morris HP (1972) Glycogen metabolism in regenerating liver and liver neoplasms. *Cancer Res* **32**, 61–66.
40 Teryukova NP, Malkova VV, Sakhenberg EI, Ivanov VA, Bezborodkina NN & Snopov SA (2018) On reprogramming of tumor cells metabolism: detection of glycogen in the cell lines of hepatocellular origin with various degrees of dedifferentiation. *Cytotechnology* **70**, 879–890.
41 Senni N, Savall M, Cabrerizo Granados D, Alves-Guerra MC, Sartor C, Lagoutte I, Gougelet A, Terris B, Gilgenkrantz H, Perret C *et al*. (2019) beta-catenin-activated hepatocellular carcinomas are addicted to fatty acids. *Gut* **68**, 322–334.
42 Calvisi DF, Wang C, Ho C, Ladu S, Lee SA, Mattu S, Destefanis G, Delogu S, Zimmermann A, Ericsson J *et al*. (2011) Increased lipogenesis, induced by AKT-mTORC1-RPS6 signaling, promotes development of human hepatocellular carcinoma. *Gastroenterology* **140**, 1071–1083.
43 Hao Q, Li T, Zhang X, Gao P, Qiao P, Li S & Geng Z (2014) Expression and roles of fatty acid synthase in hepatocellular carcinoma. *Oncol Rep* **32**, 2471–2476.

44 Che L, Paliogiannis P, Cigliano A, Pilo MG, Chen X & Calvisi DF (2019) Pathogenetic, prognostic, and therapeutic role of fatty acid synthase in human hepatocellular carcinoma. *Front Oncol* **9**.
45 Mah CY, Nassar ZD, Swinnen JV & Butler LM (2020) Lipogenic effects of androgen signaling in normal and malignant prostate. *Asian J Urol* **7**, 258–270.
46 Yang Z, Qin W, Chen Y, Yuan B, Song X, Wang B, Shen F, Fu J & Wang H (2018) Cholesterol inhibits hepatocellular carcinoma invasion and metastasis by promoting CD44 localization in lipid rafts. *Cancer Lett* **429**, 66–77.
47 Liu H, Dong H, Robertson K & Liu C (2011) DNA methylation suppresses expression of the urea cycle enzyme carbamoyl phosphate synthetase 1 (CPS1) in human hepatocellular carcinoma. *Am J Pathol* **178**, 652–661.
48 Wasfy RE & Shams Eldeen AA (2015) Roles of combined glypican-3 and glutamine synthetase in differential diagnosis of hepatocellular lesions. *Asian Pac J Cancer Prev* **16**, 4769–4775.
49 Deng Y, Li X, Li X, Zheng Z, Huang W, Chen L, Tong Q & Ming Y (2018) Corilagin induces the apoptosis of hepatocellular carcinoma cells through the mitochondrial apoptotic and death receptor pathways. *Oncol Rep* **39**, 2545–2552.
50 Hamilton SR & Aaltonen LA (2000) Pathology and Genetics of Tumours of the Digestive System. IARCPress, Lyon.
51 Cox J & Mann M (2008) MaxQuant enables high peptide identification rates, individualized p.p.b.-range mass accuracies and proteome-wide protein quantification. *Nat Biotechnol* **26**, 1367–1372.
52 Gielisch I & Meierhofer D (2015) Metabolome and proteome profiling of complex I deficiency induced by rotenone. *J Proteome Res* **14**, 224–235.
53 Cox J, Neuhauser N, Michalski A, Scheltema RA, Olsen JV & Mann M (2011) Andromeda: a peptide search engine integrated into the MaxQuant environment. *J Proteome Res* **10**, 1794–1805.

Supporting information

Additional supporting information may be found online in the Supporting Information section at the end of the article.
Table S1. Gene expression signatures of the tumors.